Fading Losses on the LCRD Free-Space Optical Link due to Channel Turbulence

Bruce Moision, Sabino Piazzolla, Jon Hamkins

Jet Propulsion Laboratory, California Institute of Technology,
4800 Oak Grove Dr., Pasadena, CA 91109

ABSTRACT

The Laser Communications Relay Demonstration (LCRD) will implement an optical communications link between a pair of Earth terminals via an Earth-orbiting satellite relay. Clear air turbulence over the communication paths will cause random fluctuations, or fading, in the received signal irradiance. In this paper we characterize losses due to fading caused by clear air turbulence. We illustrate the performance of a representative relay link, utilizing a channel interleaver and error-correction-code to mitigate fading, and provide a method to quickly determine the link performance.

Keywords: optical communications, fading, relay channel

1. INTRODUCTION

The Laser Communications Relay Demonstration (LCRD) will (initially) consist of a pair ground stations communicating through a relay satellite in a GEO orbit. The ground stations will be located at the NASA/JPL Table Mountain Facility in California and the NASA White Sands Facility in New Mexico. A signal will be transmitted from a telescope at one of these terminals to the satellite. On board the satellite, a modem will demodulate the signal and transmit the demodulated data back to either the transmitting ground station or the second ground station. The relay link between the two stations will experience the effects of optical turbulence both for the uplink and the downlink. Clear air turbulence over the path will cause random fluctuations, or fading, in the received signal irradiance at each receiver. These fluctuations cause a loss in performance relative to a link without fading. The LCRD system will mitigate fading losses by introducing temporal diversity with a channel interleaver and utilizing a DVB-S2 error correction code (ECC) to provide coding gain over the fades. In this paper we characterize the performance of this link.

The paper is organized as follows. In Section 2 we describe the channel model. In Section 3 we describe the generation of the fading time series. In Section 4 we illustrate the performance of a representative link, and illustrate a methodology to quickly and accurately predict the link behavior.

2. COMMUNICATIONS CHANNEL MODEL

Figure 1 illustrates a block diagram of the communications channel model. A block of k information bits $\{a_0, a_1, \ldots, a_{k-1}\}, a_i \in \{0,1\}$ are encoded by a DVB-S2 error-correction-code (ECC) to produce a block of n coded bits $\{x_0, x_1, \ldots, x_{n-1}\}, x_i \in \{0,1\}$. The coded bits are interleaved with a convolutional interleaver with N rows and delays a multiple of B (coded) bits. We denote the interleaved bit stream, the output of the convolutional interleaver, as $\ldots, \tilde{x}_0, \tilde{x}_1, \ldots, \tilde{x}_i, \ldots$. These bits are modulated with differential-phase-shift-keying (DPSK) and transmitted to the satellite over the free-space uplink channel. On the satellite, the signal is demodulated, producing estimates of the coded bits. The bit estimates are made bit-by-bit and do not utilize the redundancy of the ECC. This bit stream (formed from the estimates of the transmitted bits $\tilde{x}$) is modulated with DPSK and transmitted to a ground receiver over the free-space downlink channel. At the ground receiver, the bits are demodulated producing log-likelihood-ratios (llrs) $\tilde{\lambda}_i = \log(p(d_i|\tilde{x}_i = 0)/p(d_i|\tilde{x}_i = 1))$ where d_i is the

 Government sponsorship acknowledged. Send correspondence to bmoision@jpl.nasa.gov. The research described in this publication was carried out by the Jet Propulsion Laboratory, California Institute of Technology, under a contract with the National Aeronautics and Space Administration

output of the DPSK receiver corresponding to coded bit $\tilde{x}_i$. The llrs are de-interleaved, and sent to the DVB-S2 decoder which produces estimates of the information bits. In the following sections we provide models for each of these blocks.

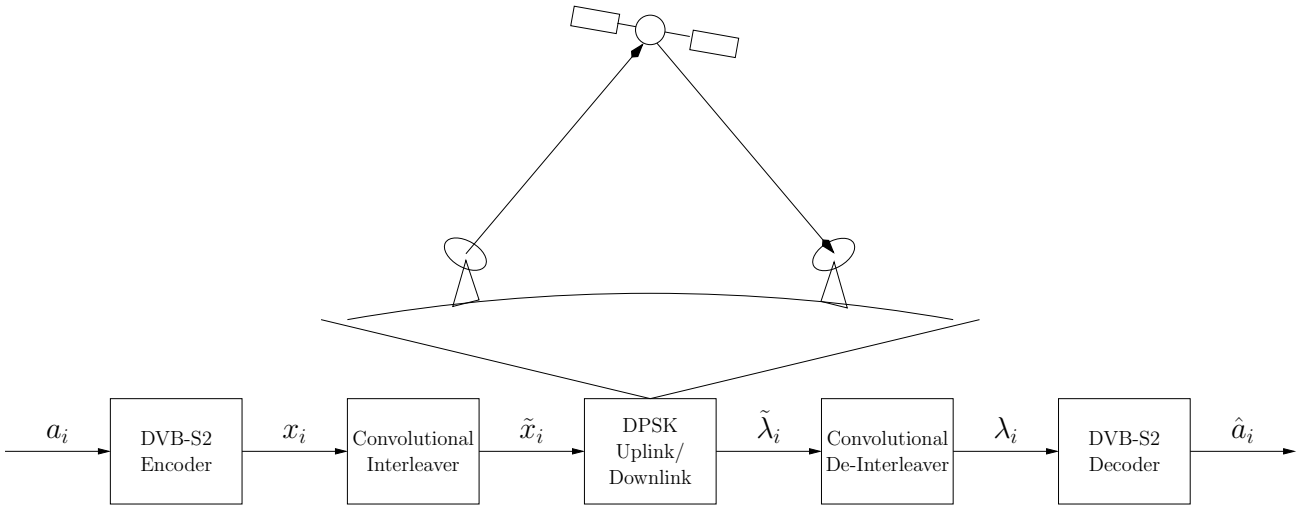

Figure 1. The Communications Relay Channel Model

2.1 DPSK Uplink/Downlink

We start by describing the physical layer and move out from there. We first treat the uplink channel. The downlink channel model is identical. The coded bits are modulated with optical binary DPSK. In DPSK, a series of optical pulses is transmitted, each with the same frequency and pulse shape, and either the same phase as the previous pulse, or a phase shift of π. The phase of the ith pulse is shifted for $\tilde{x}_i = 1$ and not shifted for $\tilde{x}_i = 0$. In general, DPSK refers to a family of modulations in which M phases are allowed.[1] Here we use it to refer to binary DPSK.

An ideal receiver for optical DPSK includes an amplifier, filter, and delay-line interferometer. The quantum limit of the noise figure for an ideal amplifier is 3 dB, and noise figures close to 3 dB have been achieved with some erbium-doped fiber amplifiers.[2] In the idealized model, the dominant source of noise is Amplified Spontaneous Emission (ASE) noise from the optical amplifier. We assume Gaussian statistics for the ASE field, and no noise from the non-amplifier parts of the channel. In this way, performance can be characterized solely as a function of the intensity of signal photons incident on the amplifier.

After the amplifier, the light signal enters an optical filter, which eliminates noise that is not at the frequency and polarization of the signal. In addition, the filter matches the temporal intensity profile of the pulse (e.g., a Gaussian shape). Following the filter, the light signal is split into two equal-intensity components, one of which enters a delay-line of one symbol period. These two fields enter an interferometer, which produces intensity outputs at a *sum* port and a *difference* port. These port outputs are sent to photodetectors, and a difference voltage is formed.

Let S denote the value of the output of the port which contains the signal (the sum port, when there is no phase shift), and N denote the output of the other port. The probability density function (pdf) of S and N are given by[3]

$$p_S(I) = \frac{2}{\gamma} \exp\left[-\frac{2(I+I_s)}{\gamma}\right] I_0\left(\frac{4}{\gamma}\sqrt{II_s}\right) \tag{1}$$

$$p_N(I) = \frac{2}{\gamma} \exp\left[-\frac{2I}{\gamma}\right] \tag{2}$$

where

$$\begin{aligned}\gamma &= \text{noise power after amplifier}\\ I_s &= \text{signal intensity at amplifier input}\\ I_0 &= \text{modified zero-order Bessel function of the first kind}\end{aligned}$$

Assuming an ideal amplifier with large gain G, we may replace I_s/γ by N_u, the mean number of photons received per channel use on the uplink,[3] where a channel use corresponds to the transmission of one pulse. Letting $y = I/\gamma$, we may rewrite (1) and (2) as

$$p_S(y) = 2e^{-2(y+N_p)} I_0\left(4\sqrt{yN_p}\right) \tag{3}$$

$$p_N(y) = 2e^{-2y} \tag{4}$$

Note that $dy = dI/\gamma$, so that the factor $1/\gamma$ is absorbed in the rescaled pdf.

Let $D = S - N$ denote the difference of the signal and noise port outputs. Then the pdf of D is the cross-correlation

$$\begin{aligned}p_D(d) &= \int_0^\infty p_S(y)p_N(y-d)dy\\ &= 4\int_0^\infty e^{-2(2y-d+N_p)} I_0\left(4\sqrt{yN_p}\right) dy\end{aligned} \tag{5}$$

We have restricted the lower limit to zero because $p_S(y) = 0$ for $y < 0$.

In the demodulator, each bit is mapped 1-1 to channel pulses, and a bit error is made when $D < 0$. This happens with probability

$$p_u = \int_{-\infty}^0 p_D(y)dy \tag{6}$$

By substituting (5) into (6), we obtain an expression that is solely a function of N_u. In fact, by manipulating suitable Marcum Q-functions, (6) can be shown to simplify to:[3]

$$\frac{1}{2}e^{-N_u} \tag{7}$$

Due to clear air turbulence, the mean received photons per channel use fluctuates randomly. Letting v_iN_u denote the mean photons per pulse for the ith channel use on the uplink, the probability that the ith bit is received in error on the satellite is given by

$$\frac{1}{2}e^{-v_iN_u} \tag{8}$$

The estimated bit stream on the flight terminal is then modulated and transmitted to the ground terminal using DPSK. Using the same model for the DPSK ground receiver as was used for the uplink receiver, and letting w_iN_d denote the mean photons per pulse for the ith channel use on the downlink, the probability that the ith bit is received in error after passing through the relay and being received on the ground is

$$p_i(w_i, v_i) = \frac{1}{2}e^{-v_iN_u}\left(1 - \frac{1}{2}e^{-w_iN_d}\right) + \frac{1}{2}e^{-w_iN_d}\left(1 - \frac{1}{2}e^{-v_iN_u}\right) \tag{9}$$

Throughout we assume that N_u, N_d are constant, and that v_i, w_i are mean one, independent random processes. The paired uplink and downlink then reduce to a time-varying binary-symmetric-channel (BSC) where the ith bit has crossover probability, or error-probability, given by (9)

2.2 Convolutional Interleaver/De-Interleaver

The received signal power fluctuates due to turbulence with a coherence time on the order of tens of milliseconds. The time it takes to transmit a codeword of bits is on the order of tens of microseconds, hence the fading is essentially constant over the duration of a codeword. If a fade drops the error-rate below the error-correction capability of the ECC, the codeword will be unrecoverable. In the LCRD system, this impact of fading is mitigated by introducing a channel interleaver into the signal stream. The interleaver spreads the coded bits that map to one codeword over a long period of time, so that the collection of bits from one codeword are affected by a number of uncorrelated fades. In this way bursts of errors are spread out. For a sufficiently long interleaver, we can think of each codeword as seeing, on average, the same number of errors over the channel. In this way any one codeword is not overwhelmed with errors, a larger fraction of codewords is recoverable, and the system performance is improved.

The LCRD interleaver is implemented as a convolutional interleaver, illustrated in Figure 2. A convolutional interleaver is used because it provides greater spreading than a block interleaver with the same memory. The convolutional interleaver consists of N rows of shift registers of length $0, B, 2B, \ldots, (N-1)B$, and operates as follows. Each register contains one coded bit. Suppose, as illustrated in Figure 2, the input and output switches are set to the first row of the interleaver, and bit x_0 is to be written. This bit passes through the interleaver, and the switches move to the second row. Then bit x_1 is written to a delay line of length B, and the delayed bit is read out. The switches proceed to the N-row, and then come back to the first row.

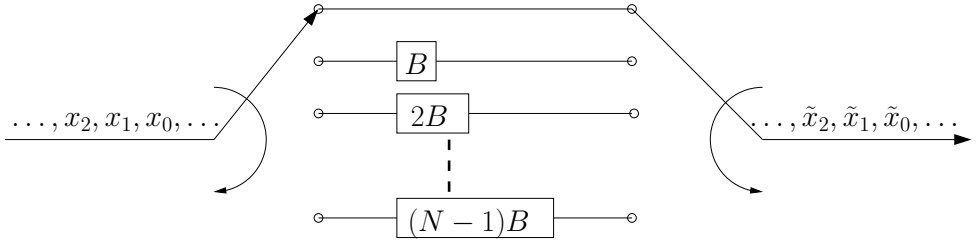

Figure 2. A Convolutional Interleaver

Figure 3 illustrates the spreading of a codeword induced by the interleaver. We can visualize the operation of the interleaver as writing the data columnwise, as in a block-interleaver, and then shifting the rows by B-bits relative to one another prior to reading them out, also columnwise. In this diagram we put the uplink fading coefficients corresponding to one codeword in place of the bits to emphasize that the purpose is to distribute the fading coefficients (each bit is affected by a pair of coefficients (v_i, w_i)-we put one only to simplify notation). Adjacent bits in the input at separated by NB (or $NB(N-1)-N$) symbols in the transmitted stream. The collection of symbols mapping to a codeword span a duration of $N(N-1)B + N_{cw} \approx N(N-1)B$ bits, where N_{cw} is the number of coded-bits in a codeword. In the LCRD interleaver, a codeword is spread over $T_I \approx 0.87$ seconds. Coherence times of the fading processes are typically on the order of 10s of milliseconds, and a codeword typically sees on the order of tens of uncorrelated samples of the fading process.

2.3 DVB-S2 Error Correction Code

The DVB-S2 codes, see, e.g.,,[4] have numerous rates and lengths. Each standard code is a serial concatenation of an outer, high-rate BCH code and an inner, lower-rate low-density parity-check (LDPC) code. The LDPC code does most of the heavy lifting in terms of error mitigation, and the BCH code is used for minor clean-up, to guarantee that no low-weight error patterns will go uncorrected. The LCRD link will use a DVB-S2 code with output and input length $(n, k) = (64800, 32208)$. The outer BCH encoder takes in $32,208$ bits and produces $32,400$ BCH-encoded bits. Next, the LDPC encoder takes the $32,400$ bits and produces $64,800$ LDPC-encoded bits. The decoding algorithm is iterative. In numerical results, we allow a maximum of 50 iterations, and terminate iterations when the parity of the ECC is satisfied. All numerical results are for a floating-point implementation of the decoder. The input to the decoder is the log-likelihood-ratio (LLR)

$$\lambda_i = \log\left(\frac{p(d_i|x_i=0)}{p(d_i|x_i=1)}\right)$$

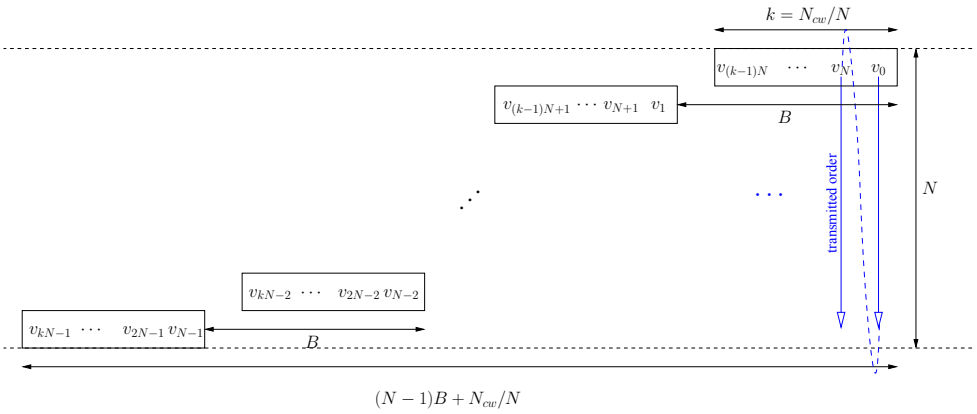

Figure 3. Interleaved Symbols

where $p(d_i = 0|x_i = 0) = p(d_i = 1|x_i = 1) = 1 - p_{e,i}$. Implicit in this LLR is the assumption that the receiver has perfect knowledge of $p_{e,i}$. We take this to be a reasonable assumption as the received power is slowly time varying (on the order of milliseconds) relative to the symbol rate (on the order of nanoseconds), so that the error rate may be learned by observing known patterns periodically inserted in the data stream.

3. POWER FLUCTUATIONS DUE TO TURBULENCE

The effects of optical turbulence will manifest themself in a different fashion at the flight terminal (uplink) and at the ground terminal (downlink). The signal irradiance incident on the flight terminal will be characterized by a relatively large dynamic range as well as other forms of loss due to beam broadening and the atmospheric Strehl ratio.[5] These uplink effects can be mitigated at the transmitter by using a tip-tilt mirror that tracks the angle of arrival of the downlink beam and compensates for it. Fading of the downlink signal is mitigated by aperture averaging of the collection area of the telescope. For the large aperture ground telescope, the ratio of the aperture diameter (D) to the atmospheric coherence length (r_o) is much larger than unity ($D/r_o \gg 1$), implying that unless adaptive optics technology is used at the ground station, phase information of the DPSK modulated signal will be lost. Therefore, the plan is to have both LCRD ground stations equipped with adaptive optics systems.[6]

As a case study for the LCRD DPSK relay links, we consider the case of a relay between the White Sands ground station (uplink) to the Table Mountain ground station (downlink). We assume the satellite is in a GEO position around 63° W of longitude, which leads to the elevation angles for the two ground terminals of 30° for the White Sands ground station and 20° for the Table Mountain ground station.

To understand and characterize the relay performance it is necessary to have a time series of the irradiance at the flight terminal and at the ground station. To do so we simulated the uplink and downlink beam time dynamics using waveoptics based software. The wavelength for the relay link is 1550 nm. The optical turbulence strength at Table Mountain was represented by a profile of the air index of refraction structure index (Cn^2) giving an atmospheric coherence length of 5.2 cm (with reference to a wavelength of 500nm at zenith). The wind profile was described by a Bufton model[7] with a ground speed of 2.3 m/s. For the uplink, the atmospheric coherence length at White Sands was 6 cm (with reference to a wavelength of 500 nm at zenith), while the ground wind speed was 4 m/s. Notice that atmospheric coherence length and wind speed values used here are approximately their corresponding median values. The uplink beam is modeled as a Gaussian beam with 16μrad full divergence. We assume no tip/tilt mirror compensation on the uplink beam. Adaptive optics drop-out effects were not included in the downlink. In these waveoptics simulations the atmosphere was divided in ten layers of equal turbulence strength and modified versions of the Hufnagel-Valley model of the vertical profile of the air index of refraction structure index[8] were used to model the turbulence at the Table Mountain and White Sands ground terminals.

Results of the waveoptics simulations are represented in the Figure 4 where the fluctuations of the normalized signal fluxes for downlink and uplink are represented over two seconds of time span (for numerical performance

results a 10 second time series was used to capture a longer realization of the random process). The sampling time was 1 ms.

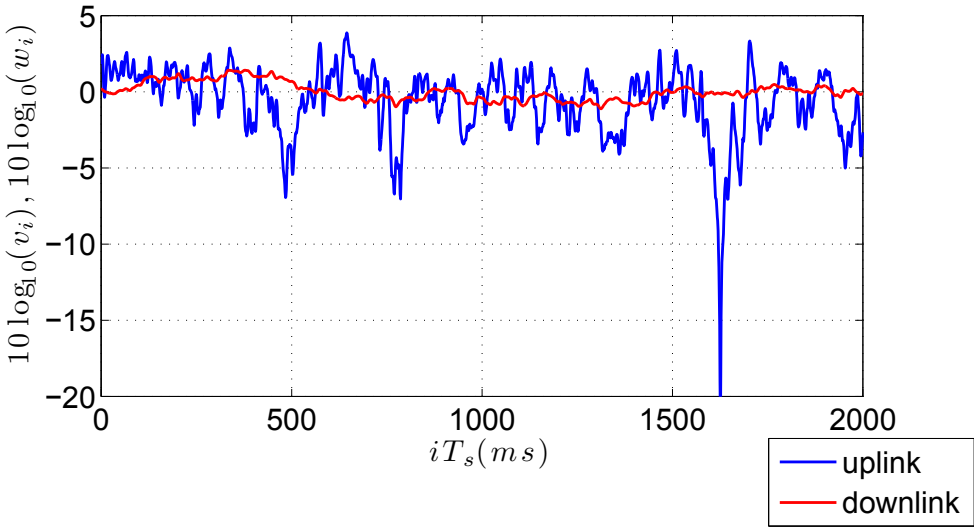

Figure 4. Uplink and downlink time series of the normalized signal simulated by waveoptics software. Downlink fading is greatly reduced by the aperture averaging (D=1m) of the ground telescope.

Figure 4 shows a large difference of the fading (scintillation) between the uplink and downlink signal. This difference is due to the fact that (1) for the uplink the optical turbulence is near to the laser source resulting in a larger scintillation index of the signal at the flight terminal,[9] and (2) the scintillation of the downlink signal is greatly reduced by the aperture averaging effect[10] of the aperture telescope to be used at the Table Mountain Facility ($D = 1$ m). We obtained a scintillation index of $\sigma^2_{I,u} = 0.163$ for the uplink and $\sigma^2_{I,d} = 0.014$ for the downlink, where the scintillation index variance of the time series normalized to have mean one. Histograms of the uplink and downlink series are illustrated in Figure 5. The downlink signal is experiencing a regime of relatively weak scintillation, such that the statistics of the variation of the downlink signal can be described relatively well by a lognormal distribution.[9] We see from Figure 5 that the variation of uplink signal is better modeled as gamma-gamma distributed (as opposed to lognormal) particularly in modeling the lower tail of the statistics associated with large fading events.

The scintillation index reflects the magnitude of the signal variances. The performance is also affected by the temporal variations. This is reflected in the coherence times of the processes, $T_{coh,u}, T_{coh,d}$, which is the time it takes the time series to become uncorrelated, a measure of the speed of variations of the time series. In this work the coherence time is defined as the 1/e-width of the autocorrelation functions of the time series. Figure 3.3 presents the autocorrelation function histogram concerning the downlink signal with its lognormal fit. Table 1 summarizes main parameters of the relay link under consideration.

	Downlink	Uplink
Scintillation Index	0.014	0.163
Coherence Time	10 ms	17 ms
Atmospheric Coherence Length at 500 nm at Zenith	5.2 cm	6.0 cm
Ground Wind Speed	2.3 m/s	4.0 m/s
Elevation Angle	20	30
Wavelength	1550 nm	1550 nm

Table 1. Relay Link Parameters

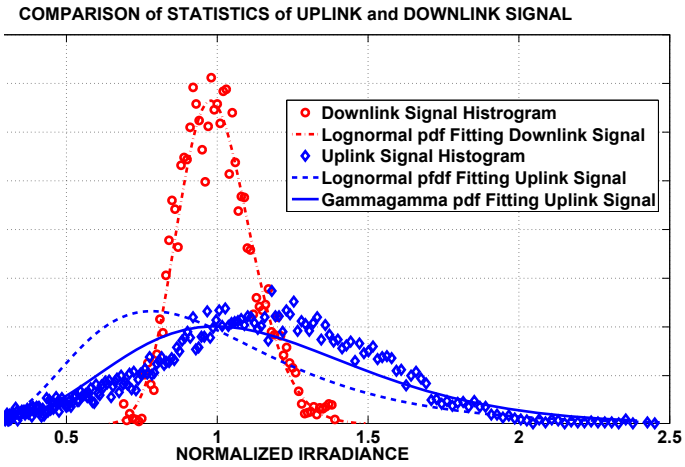

Figure 5. Comparison of the uplink and downlink signal irradiance statistics. Downlink signal can be adequately described by a lognormal probability distribution funcion. Because of larger scintillation index, the uplink signal irradiance statistics was better described by a gammagamma pdf.

4. RELAY PERFORMANCE

Utilizing the time series described in Section 3 and the channel model described in Section 2, we generate the threshold curve illustrated in Figure 6, which illustrates the pairs of points (N_u, N_d) where the word error rate (WER) of the ECC is 10^{-4}. We refer to this as a threshold curve since all points with (N_u, N_d) greater than the curve have WER$< 10^{-4}$, and all points less than the curve have WER$> 10^{-4}$. We take this as the threshold determining acceptable link closure. When the downlink power is large, the decision on the flight terminal is perfectly reproduced on the ground, and the performance approaches the asymptote we would achieve by transmitting over the uplink only. Similarly, at sufficiently large uplink power, the performance approaches the limit of the downlink. Let N_u^* and N_d^* denote these asymptotes. In Figure 6 they are illustrated by dashed lines and fall at $10\log_{10}(N_u^*) = 3.3$ dB-photons/channel-use and $10\log_{10}(N_d^*) = 2.7$ dB-photons/channel-use. If the fading processes may be modeled as lognormal, the asymptotes may be accurately predicted as[11]

$$10\log_{10}(N_u^*) \approx 2.3 + 2.2\sigma_u^2 + 16\sigma_u/\sqrt{T_I/T_{coh,u}} = 3.4 \text{ dB-photons/channel-use}$$

$$10\log_{10}(N_d^*) \approx 2.3 + 2.2\sigma_d^2 + 16\sigma_d/\sqrt{T_I/T_{coh,d}} = 2.5 \text{ dB-photons/channel-use}$$

where, $\sigma_u^2 = \log(1+\sigma_{I,u}^2), \sigma_d^2 = \log(1+\sigma_{I,d}^2)$, and, recall, $T_I = 0.87$ sec is the duration over which a codeword is spread. Here we see a good prediction, although we do not claim this approximation is good when the processes are not lognormal. Nonetheless, it provides a quick understanding of how the losses factor, which we expect to roughly hold. The first term, 2.3 dB, is the threshold in the absence of fading. The second term, $2.2\sigma^2$, is a loss in the fading capacity (to be described later) which is linear in the scintillation index. The third term, $16\sigma/\sqrt{T_I/T_{coh,u}}$, captures losses due to finite-interleaving (relative to an infinite-duration interleaver), which we see may be decreased by increasing the interleaver duration.

On a one-way link one would compute the link margin as the difference between the received power and the minimum power required to close the link. On the relay link we have a continuum of pairs of margins, since the uplink margin is a function of the downlink margin, and vice versa. That is to say, the power one has in excess of the minimum required to close the link on the uplink depends on the quality of the downlink, and, hence, the downlink margin. Let (N_u^r, N_d^r) denote the received uplink and downlink photon flux rates. Suppose $(10\log_{10}(N_u^r), 10\log_{10}(N_d^r)) = (12, 10)$, illustrated as a point in Figure 6. Here we have positive margins. Figure 7 shows the collection of pairs $(N_u^r - N_u, N_d^r - N_d)$ where (N_u, N_d) is a point on the threshold curve. This margin curve illustrates the collection of margins for this given received power.

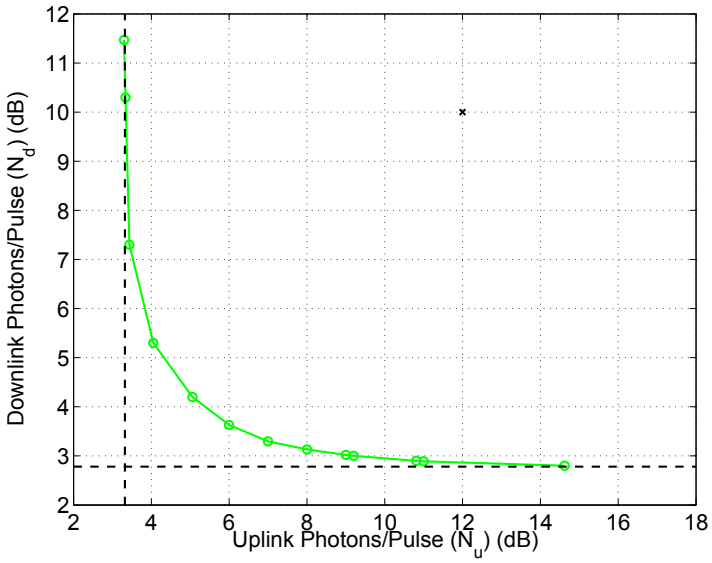

Figure 6. Relay Transfer Curve

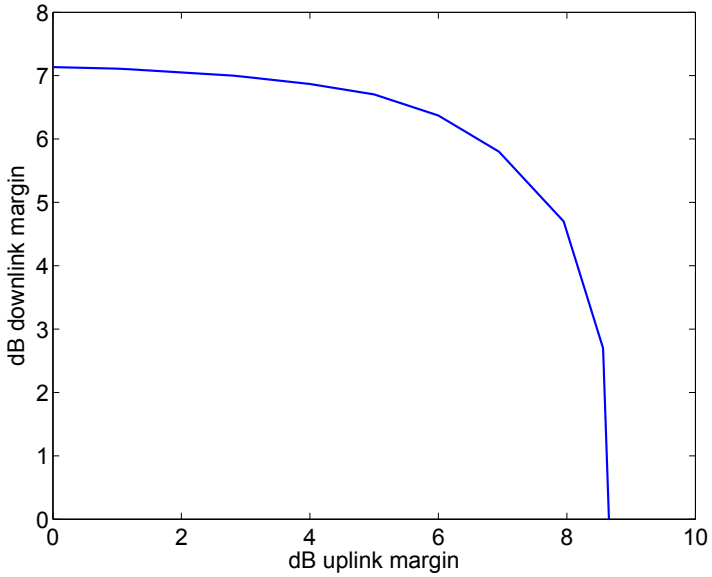

Figure 7. Relay Margin Curve Corresponding to Figure 6 with $(10\log_{10}(N_u^r), 10\log_{10}(N_d^r)) = (12, 10)$ dB-photons/channel-use

4.1 Predicting the Relay Performance

One direct method to obtain the threshold curve illustrated in Figure 6 is to fix an uplink power N_u and measure the WER as a function of N_d via simulation of the coded system performance, searching for the threshold WER= 10^{-4}. This, however, can be very time consuming. In this section we provide a method to quickly and accurately predict the threshold curve, extending results for one-way links from[11,12]

We may bound the performance of the coded relay via the relay channel capacity. The channel capacity bounds the rate at which one can transmit data over the channel with arbitrarily small error rate. For a BSC with a constant error rate the channel capacity is given by

$$C(p_e) = 1 + p_e \log_2(p_e) + (1 - p_e) \log_2(1 - p_e) \text{ bits/channel-use} \tag{10}$$

For a fading channel with a randomly time-varying error rate where the receiver has knowledge of the channel state (the receiver knows (v_i, w_i) exactly) the capacity is given by

$$C_f = E_{V,W}[C(p_e(V, W))]$$

The fading channel capacity can be achieved in the limit of infinitely long blocklength codes. Any practical, finite-length code will have performance bounded away from the capacity. In particular, in the presence of fading, the code performance in limited because each codeword sees only a finite collection of fading coefficients. Let $\{v_0, v_1, \ldots, v_{N_f}\}$ and $\{w_1, w_2, \ldots, w_{N_f}\}$ denote the collection of coefficients mapping to one codeword. That codeword sees an instantaeous snapshot of the channel defined by the finite set of fading coefficients. If the channel were fixed for all time and represented by that set of coefficients, it would have (instantaneous) capacity

$$C_i = \frac{1}{N_f} \sum_{j=1}^{N_f} C(p_{e,j})$$

Define an outage as the event that the instantaneous capacity falls below the information rate, with probability

$$p_{out} = P(R_b < C_i)$$

With high probability, if the instantaneous capacity falls below the information rate, the codeword will be received in error. The codeword error rate, P_w, in fading is hence well approximated as

$$\begin{aligned} P_w &= P(R_b < C_i, \text{decoding error}) + P(R_b \geq C_i, \text{decoding error}) \\ &= P(\text{decoding error}|R_b < C_i)P(R_b < C_i) + P(\text{decoding error}|R_b \geq C_i)P(R_b \geq C_i) \\ &\approx p_{out} + (1 - p_{out})P(\text{decoding error}|R_b \geq C_i) \\ &\approx p_{out} + P(\text{decoding error}|R_b \geq C_i) \end{aligned}$$

The threshold for a target P_w occurs at an offset to the outage probability. We find that the increase in power relative to the outage threshold to achieve a WER equal to the outage threshold is approximately the same in the presence and absence of fading. That is, if we require 0.525 dB increase relative to the outage (capacity) threshold in the absence of fading, we will require approximately the same offset in the presence of fading.

Let $(\tilde{N}_u, \tilde{N}_d)$ denote the pairs of uplink and downlink powers achieving $p_{out} = 10^{-4}$. Figure 8 illustrates $(\tilde{N}_u, \tilde{N}_d)$. We obtain a good approximation of the coded performance threshold by offsetting this curve such that it agrees in the asymptotes with eh the measured (or calculated) asymptotes (N_u^*, N_d^*). This offset prediction is also illustrated in Figure 8. Computing the threshold in this manner is much more efficient than a direct simulation.

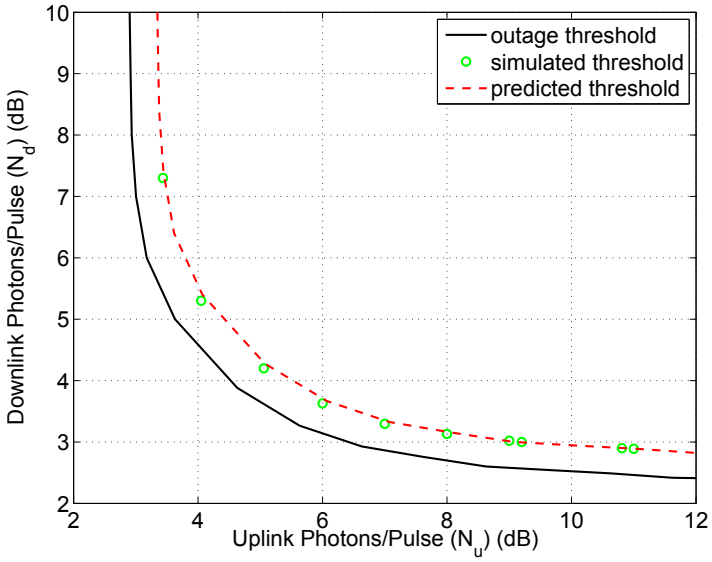

Figure 8. Code Threshold, Outage Threshold, and Code Threshold predicted from Outage Threshold

5. CONCLUSIONS

The LCRD relay link will be affected by clear air turbulence on both the uplink and downlink paths. These fading time series may be modeled with waveoptics simulations. For representative LCRD links, the downlink fading time series is well modeled as lognormally distributed and the uplink fading series is reasonably well modeled as gamma-gamma distributed. The performance of the coded, interleaved, and DPSK modulated relay channel is characterized by a collection of pairs of uplink and downlink powers that satisfy a definition of link closure (which we here took to be a codeword error rate of 10^{-4}). The notion of a margin on the relay link is similarly captured as a collection of pairs given by the excess uplink and downlink received power relative to the uplink and downlink required power. Characterizing a threshold curve consisting of a collection of operating points via simulation of the coded system may be prohibitively complex. However, one may quickly and simply compute the outage probability threshold and, by shifting it to align with the coded system asymptotes, obtain a good approximation to the coded threshold curve. In this manner a large number of links may be quickly characterized.

ACKNOWLEDGMENTS

Thanks to Baris Erkmen for discussions on information rates on fading channels.

REFERENCES

[1] Qu, S. and Sheikh, A., "Analysis of channel capacity of M-ary DPSK and D^{2}PSK with time-selective Rician fading," in [*IEEE 43rd Vehicular Technology Conference*], (May 1993).

[2] Becker, P., Olsson, N., and Simpson, J., [*Erbium-doped fiber amplifiers: fundamentals and technology*], vol. 1, Academic Pr (1999).

[3] Chinn, S., Boroson, D., and Livas, J., "Sensitivity of optically preamplified DPSK receivers with Fabry-Perot filters," *J. Lightwave Technol.* **14** (Mar. 1996).

[4] ETSI, *Digital Video Broadcasting (DVB): Second generation framing structure, channel coding and modulation for Broadcasting, Interactive Services, News Gathering and other broadband satellite applications*, en 302 307 ed. (June 2004). V1.1.1.

[5] Andrews, L. C., Phillips, R. L., Sasiela, R. J., and Parenti, R. R., "Strehl ratio and scintillation theory for uplink Gaussian-beam waves: beam wander effects," *Opt. Eng.* (45) (2006).

[6] Jr., L. C. R., Page, N. A., Burruss, R., Truonga, T. N., Dew, S., and Troy, M., "Conceptual design of the adaptive optics system for the laser communication relay demonstration ground station at Table Mountain," in [*Proceedings of the SPIE*], (2013).

[7] Bufton, J. A., "Comparison of vertical profile turbulence structure with stellar observations," *Applied Optics* **12**(8) (1973).

[8] Beland, R., [*The Infrared and Electro-Optical Systems Handbook*], vol. 2, ch. Propagation Through Atmospheric Optical Turbulence, SPIE, Bellingham, WA (1993).

[9] Andrews, L. C. and Phillips, R. L., [*Laser Beam Propagation through Random Media*], SPIE, 2 ed. (2005).

[10] Yura, H. T. and McKinley, W. G., "Aperture averaging of scintillation for space-to-ground optical communication applications," *Applied Optics* **22**(11) (1983).

[11] Moision, B., Shambayati, S., and Wu, J., "An optical communications link design tool for long-term mission planning for deep-space missions," in [*IEEE Aerospace Conference*], (March 2012).

[12] Barron, R. J. and Boroson, D. M., "Analysis of capacity and probability of outage for free-space optical channels with fading due to pointing and tracking error," in [*Proceedings of SPIE*], **6105**, Proceedings of the SPIE (March 2006).